AIP | Physics of Plasmas

Effects of q-profile structure on turbulence spreading: A fluctuation intensity transport analysis

S. Yi, J. M. Kwon, P. H. Diamond, and T. S. Hahm

Citation: Physics of Plasmas (1994-present) **21**, 092509 (2014); doi: 10.1063/1.4896059
View online: http://dx.doi.org/10.1063/1.4896059
View Table of Contents: http://scitation.aip.org/content/aip/journal/pop/21/9?ver=pdfcov
Published by the AIP Publishing

Articles you may be interested in

Characterizing turbulent transport in ASDEX Upgrade L-mode plasmas via nonlinear gyrokinetic simulations
Phys. Plasmas **20**, 122312 (2013); 10.1063/1.4858899

Effect of secondary convective cells on turbulence intensity profiles, flow generation, and transport
Phys. Plasmas **19**, 112506 (2012); 10.1063/1.4767652

Experimental study of parametric dependence of electron-scale turbulence in a spherical tokamaka)
Phys. Plasmas **19**, 056125 (2012); 10.1063/1.4719689

Suppressing electron turbulence and triggering internal transport barriers with reversed magnetic shear in the National Spherical Torus Experimenta)
Phys. Plasmas **19**, 056120 (2012); 10.1063/1.4718456

Role of nonlinear toroidal coupling in electron temperature gradient turbulencea)
Phys. Plasmas **12**, 056125 (2005); 10.1063/1.1894766

This article is copyrighted as indicated in the article. Reuse of AIP content is subject to the terms at: http://scitation.aip.org/termsconditions. Downloaded to IP: 132.239.66.163 On: Wed, 14 Jan 2015 19:24:19

Effects of q-profile structure on turbulence spreading: A fluctuation intensity transport analysis

S. Yi,[1] J. M. Kwon,[1] P. H. Diamond,[1,2] and T. S. Hahm[3]
[1]National Fusion Research Institute, Eoeun-dong, Yuseong-gu, Daejeon 305-333, South Korea
[2]Center for Astrophysics and Space Sciences and Department of Physics, University of California San Diego, La Jolla, California 92093-0429, USA
[3]Department of Nuclear Engineering, Seoul National University, Seoul 151-744, South Korea

(Received 10 July 2014; accepted 5 September 2014; published online 18 September 2014)

This paper studies effects of q-profile structure on turbulence spreading. It reports results of numerical experiments using global gyrokinetic simulations. We examine propagation of turbulence, triggered by an identical linear instability in a source region, into an adjacent, linearly stable region with variable q-profile. The numerical experiments are designed so as to separate the physics of turbulence spreading from that of linear stability. The strength of turbulence spreading is measured by the penetration depth of turbulence. Dynamics of spreading are elucidated by fluctuation intensity balance analysis, using a model intensity evolution equation which retains nonlinear diffusion and damping, and linear growth. It is found that turbulence spreading is strongly affected by magnetic shear s, but is hardly altered by the safety factor q itself. There is an optimal range of modest magnetic shear which maximizes turbulence spreading. For high to modest shear values, the spreading is enhanced by the increase of the mode correlation length with decreasing magnetic shear. However, the efficiency of spreading drops for sufficiently low magnetic shear even though the mode correlation length is comparable to that for the case of optimal magnetic shear. The reduction of spreading is attributed to the increase in time required for the requisite nonlinear mode-mode interactions. The effect of increased interaction time dominates that of increased mode correlation length. Our findings of the reduction of spreading and the increase in interaction time at weak magnetic shear are consistent with the well-known benefit of weak or reversed magnetic shear for core confinement enhancement. Weak shear is shown to promote locality, as well as stability. © *2014 AIP Publishing LLC*. [http://dx.doi.org/10.1063/1.4896059]

I. INTRODUCTION

Understanding and prediction of turbulent plasma transport are crucial to achieve and sustain improved confinement states for steady state tokamaks such as ITER. Present day understanding and modeling of turbulent transport are based primarily on the following local paradigm: fluxes of physical quantities are described by diffusive or convective transport coefficients, which are determined by competition between the linear growth driven by local gradients of profiles and the $E \times B$ nonlinearity. For micro-turbulence, local, mixing-length-type models predict that the resulting transport is consistent with gyro-Bohm scaling, i.e., the diffusion coefficient is proportional to the normalized ion gyro-radius $\rho_* \equiv \rho_i/a$, where a is the minor radius. However, many observations in actual experiments disagree with the prediction of local models.[1] In addition to the breaking of the gyro-Bohm scaling, there is mounting evidence for the breakdown of the local transport model, e.g., the observation of transient transport events which occur faster than the typical global confinement time scale,[2,3] the surge of fluctuation level at the innermost radius of the radial electric field (E_r) shear layer during the H-L back-transition,[4] etc. These deviations of transport dynamics from local models are usually classified as non-local transport phenomena.

One mechanism potentially responsible for non-local phenomena is turbulence spreading, i.e., the propagation of fluctuation energy itself into a different regions by nonlinear spectral transfer.[5–11] Turbulence spreading can decouple local turbulence intensity, and thus turbulent diffusivity, from the local gradient. Such an outcome causes deviation from local transport models. In the literature, turbulence spreading is invoked to explain various non-local transport phenomena.[6,7,12–15] Spreading can reduce the turbulence intensity in the linearly unstable region and introduce additional dependence on ρ_* to the turbulence intensity.[6,7] The additional ρ_* dependence causes the resulting transport to deviate from gyro-Bohm scaling, especially for smaller devices ($a/\rho_i < 200$). Also, theoretical models employing turbulence spreading may explain the challenging experimental observations of non-locality. The fast increase of core electron temperature by peripheral perturbations[2,3] can be captured by a simple two-field model with the temperature and turbulence intensity evolution.[13,14] A meso-scale model with turbulence spreading[15] shows that a H-L back transition can be triggered by the spreading of turbulence from the core region into a E_r shear layer, which is consistent with the observation from recent experiments.[4] It is worth recalling avalanches as another, closely related, non-local mechanism. Avalanches occur in the dynamics of a marginally stable system and can play a role in non-local transport events.[16] While spreading results from spatial scattering by triads, avalanches lead to scattering via temperature gradient perturbations. In a marginally stable system, avalanches can impact the evolution of the turbulence intensity profile.

 © 2014 AIP Publishing LLC

This article is copyrighted as indicated in the article. Reuse of AIP content is subject to the terms at: http://scitation.aip.org/termsconditions. Downloaded to IP: 132.239.66.163 On: Wed, 14 Jan 2015 19:24:19

Upon recognizing the practical importance of turbulence spreading in transport processes, a subsequent question is in which conditions of plasma equilibria, turbulence spreading plays a significant role. However, the standard theoretical models of turbulence spreading have difficulty in answering this question. This is because of the following. The radial flux of turbulence energy is caused by numerous nonlinear mode-mode interactions, and determined by integrals over the turbulence spectrum, with a resonance condition in two-dimensional spectral space of poloidal and toroidal wave number. It is thus very difficult to compute analytically the radial flux of turbulence energy for cases of realistic toroidal plasmas. So, many theoretical models of turbulence spreading employ an alternative approach in which the spreading is thought of as a random walk process. In such models, turbulence spreading is usually described by a nonlinear diffusion equation of the form

$$\frac{\partial I}{\partial t} - \frac{\partial}{\partial r}\left(D_0 I \frac{\partial I}{\partial r}\right) = local\ growth/damping\ terms,$$

which involves a prescribed coefficient D_0 which, in principle, depends on the detailed plasma conditions, such as magnetic geometry and profile of mean (and zonal) flow shear. Due to this simplification, detailed studies of the dependence of turbulence spreading upon experimental conditions are formidable task and there were only a few numerical simulation studies reporting the effects of plasma conditions.[9,17,18] In order to study the inward spreading of edge turbulence toward the core plasma, Hahm *et al.* utilized a two-step structure for the ion temperature gradient where the temperature gradient value at the edge is double of that in the core.[9] They found a proportionality of the spreading speed to the ion temperature gradient, which implied that the dominant mechanism responsible for spreading is nonlinear coupling rather than the linear toroidal coupling. Wang *et al.* applied a fixed equilibrium E_r shear, and then compared the spreading extent for variable E_r shear.[18] They found that a $E \times B$ shear layer can significantly reduce turbulence spreading. In addition, they compared the turbulence propagation velocity in the cases with, and without, self-generated zonal flows, and found that the propagation velocity is significantly reduced in the presence of zonal flows.

There are many experimental results indicating the importance of equilibrium magnetic geometry for plasma transport. Magnetic shear is a critical parameter in the bifurcation of turbulent transport.[19–22] Also, magnetic shear affects the stiffness of ion temperature profile.[23,24] The magnetic shear is likely to impact turbulence spreading because it affects the radial structure of modes, and also thus the nonlinear interactions among them. In this work, motivated by the lack of previous critical studies, we systematically investigate the effects of magnetic geometry on turbulence spreading. To this end, we use a global gyrokinetic model which self-consistently handles numerous nonlinear mode-mode interactions in realistic toroidal plasmas. This work is the first systematic study of effects of the q-profile structure on spreading. We compare spreading length relative to radial correlation length and quantitatively evaluate the strength of spreading by performing a fluctuation intensity balance analysis.

A brief overview of the basics of turbulence spreading will help us to understand the forthcoming simulations and analyses. The dynamics of turbulence spreading, i.e., the spatio-temporal scattering of local turbulence intensity I is determined by the following model equation:[6,10,25,26]

$$\frac{\partial I}{\partial t} + \frac{\partial \Gamma_I}{\partial r} = \gamma[\nabla T]I - \gamma_{NL} I^2 + 2V_{ZF}\frac{\partial}{\partial r}\langle v_r v_\theta\rangle + \cdots,$$
$$\Gamma_I = -\int dr' \mathcal{K}(r,r')\frac{\partial I(r')}{\partial r}, \quad (1)$$

where flux of turbulence intensity Γ_I is expressed by a generalized turbulence intensity transfer integral, to capture non-diffusive components of the flux and/or non-local dynamics of turbulence spreading.[27] But, we assume locality in time, i.e., no memory in the nonlinear dynamics. If the width of kernel $\mathcal{K}$ is comparable to a typical radial correlation length of turbulence, the intensity flux can be reduced to local diffusion, i.e., $\Gamma_I = -D_0 I \partial I/\partial r$, where the diffusivity of turbulence energy transfer is proportional to I. The first two terms in the right hand side correspond to the local linear growth/damping and nonlinear decay, respectively. The local nonlinear damping represents the coupling of fluctuation energy to damped scales, which causes the local saturation of fluctuation levels. The third term in the right hand side of Eq. (1) describes the drain on fluctuation energy by Reynolds work which drives the zonal flow V_{ZF}. Since turbulence is self-regulated through the zonal flow, the evolution of turbulence intensity is affected by zonal flow, whose evolution is determined by[26]

$$\frac{\partial V_{ZF}}{\partial t} = -\frac{\partial}{\partial r}\langle v_r v_\theta\rangle - \mu V_{ZF},$$

where μ is the drag damping of zonal flow. The saturation level of zonal flow is given by

$$V_{ZF,0} = -\frac{1}{\mu}\frac{\partial\langle v_r v_\theta\rangle}{\partial r} \sim \frac{1}{\mu}\frac{\partial}{\partial r}\sum_{\mathbf{k}} k_r k_\theta \phi_{\mathbf{k}}^2 \sim I,$$

which is proportional to the level of turbulence. Conservation of fluctuation and flow energy implies that the zonal flow saturation level necessarily impacts the saturated turbulence intensity via

$$\left.\frac{\partial I}{\partial t}\right|_{ZF} \approx -2\mu V_{ZF,0}^2 \sim -I^2. \quad (2)$$

Furthermore, the evolution of turbulence intensity is linked to temperature evolution because turbulence drive depends on the temperature gradient. Thus, turbulence spreading and avalanching in heat transport can affect each other.

Varying q-profile structure affects not only turbulence spreading but also local growth and damping processes. The evolution of turbulence intensity is determined by the interplay between the local and spreading processes. To separate the effects of q-profile structure on spreading from contributions due local processes, the simulation conditions are

This article is copyrighted as indicated in the article. Reuse of AIP content is subject to the terms at: http://scitation.aip.org/termsconditions. Downloaded to IP: 132.239.66.163 On: Wed, 14 Jan 2015 19:24:19

TABLE I. Analogy between the analyses of fluctuation intensity transport and usual turbulent transport. Note that $\gamma_d < 0$.

	Estimation of spreading	Estimation of turbulent diffusion
Transportee	Fluctuation intensity $I = \langle \delta\phi^2 \rangle$	Temperature T, density n, toroidal flow V_φ
Steady state balance	Transfer by spreading vs. local damping, $-\partial_r[D_0 I \partial_r I] = \gamma_d I - \gamma_{NL} I^2$	Turbulent transport vs. local effective source, $-\partial_r[\chi \partial_r T] = S$
Measured quantities	Linear damping rate γ_d, turbulence saturation level I_0, and penetration depth x_0	Flux $\Gamma = \int^r S(r')dr'$ and profile gradient $\partial_r T$
Diffusivity	$D_0 I_0 \sim \lvert\gamma_d\rvert x_0^2/2$ using approximation of $\partial_r I \sim -I_0/x_0$ and $\int I dr \sim I_0 x_0/2$	$\chi = -\Gamma/\partial_r T$

carefully designed, as follows. The radial domain is divided into two regions, linearly unstable and stable zone. The unstable region is set to support identical linear instabilities and its q-profile structure does not change. In the stable region, different q-profiles are chosen to investigate their effects on turbulence spreading triggered by the same instability. Zonal flow evolution is retained, so its contribution to spreading is included in results self-consistently. A definite contribution of zonal flow is the reduction of the turbulence level in the linearly unstable region. In addition, we estimate the effects of the local damping, and extract strength of spreading by fluctuation intensity balance analysis, similar to the process of thermal diffusivity estimation from steady state energy balance in transport experiments. A comparison between the analyses of fluctuation intensity transport and usual turbulent transport is presented in Table I. (See Sec. II B for the details.)

The remainder of this paper is organized as follows: In Sec. II, we explain the numerical experiments performed using the gyrokinetic model and details of fluctuation intensity transport analysis. In Sec. III, we present results on the effects of q-profile structure on turbulence spreading. Finally, conclusions and discussion are given in Sec. IV.

II. SIMULATION MODEL AND ANALYSIS METHOD

A. Setup of numerical experiments

In this study, we use a global δf gyrokinetic particle in cell code gKPSP.[28] gKPSP solves the electrostatic gyrokinetic Vlasov-Poisson equations in toroidal geometry[29] with adiabatic electrons. More details of the simulation model can be found in Ref. 28.

In this work, the separation of local and spreading processes is essential to study the effects of q-profile structure on turbulence spreading. To facilitate the analysis, we use the following setup for gyrokinetic simulations. The radial domain is divided into two regions, an inner core and the outer region with linearly unstable and stable ion temperature (T_i) profiles of $R_0/L_{Ti} = 7.14$ and $R_0/L_{Ti} = 3.57$, respectively. The gradient of the density profile is nearly constant with $R_0/L_n \approx 2.22$. Then, we have $\eta_i = L_n/L_{Ti} = 3.22$ in the unstable core region and $\eta_i = 1.61$ in the stable outer region. Here, R_0 is the major radius, $L_{Ti}^{-1} = (dT_i/dr)/T_i$ and $L_n^{-1} = (dn/dr)/n$ are the inverse of the ion temperature and density gradient scale length, respectively. Electron temperature profile is set as the same as the ion temperature profile. Figure 1(a) shows the initial profiles of temperature and density gradients, and η_i. The profile of the ion temperature gradient is given by $R_0/L_{Ti} = 7.14[\exp(-x^4) + 1]/2$, where $x = (r/a - 0.35)/0.12$. A typical profile of the linear growth/damping rate is shown in Fig. 1(b). The linear damping rate changes as q-profile varies. Ion temperature gradient (ITG) driven turbulence is excited in the unstable core region with $0.22 < r/a < 0.48$, where the onset condition is satisfied (i.e., $\eta_i > 2.0$),[30] and spills over into the stable outer region with $r/a > 0.48$.

We consider monotonically increasing q-profiles with a polynomial form $q(r) = q_0 + q_1 r + q_2 r^2 + q_3 r^3$. Figure 2 shows the profiles used in our simulations. These q-profiles can be categorized into two sets, one set for the magnetic shear $s \equiv (r/q)(dq/dr)$ scan and the other set for the safety factor q scan. The former set is designed to provide different magnetic shear values in the stable outer region for the study of magnetic shear effects on turbulence spreading. The variation of magnetic shear entails an unavoidable variation of the q-profile, and both the q and s values will cause the changes in turbulence spreading. The latter set will be used to complement the studies with the first set by providing cases with fixed magnetic shear varying safety factor. We denote the cases in the s-scan

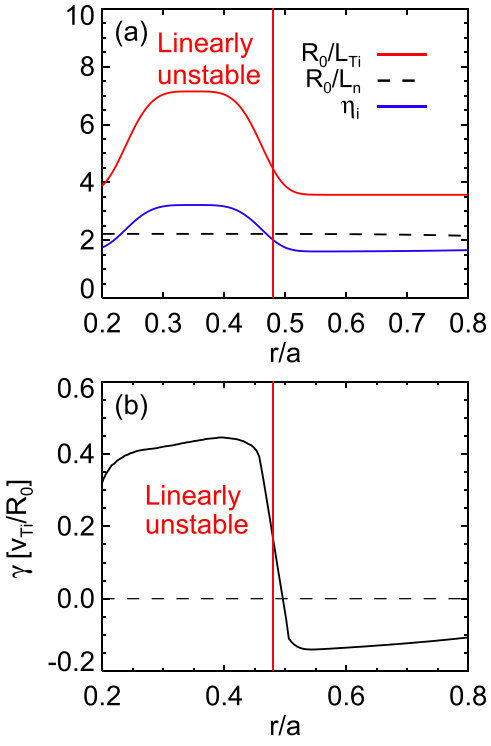

FIG. 1. (a) Initial profiles of ion temperature and density gradients, and η_i. (b) Profile of linear growth and damping rate of the case of $s = 0.7$.

This article is copyrighted as indicated in the article. Reuse of AIP content is subject to the terms at: http://scitation.aip.org/termsconditions. Downloaded to IP: 132.239.66.163 On: Wed, 14 Jan 2015 19:24:19

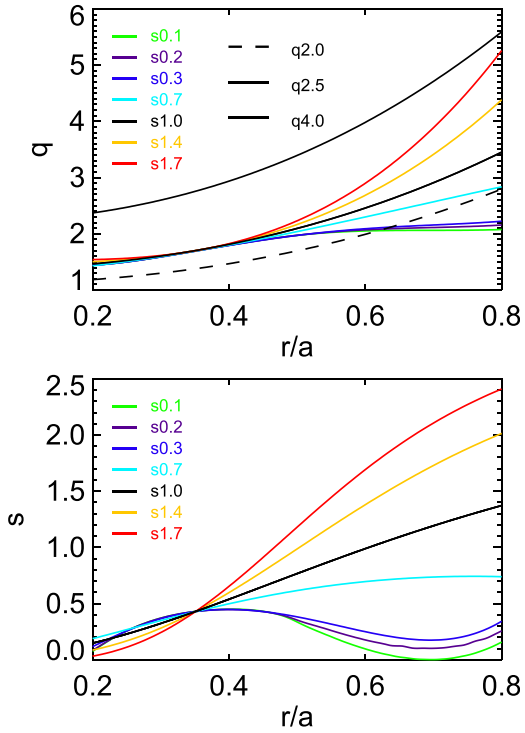

FIG. 2. Radial profiles of (a) safety factor q and (b) magnetic shear s. The q-profiles in s-scan (the solid lines) have the same values of $q = 1.7$ and $s = 0.43$ at $r/a = 0.35$.

(q-scan) with the values of magnetic shear (safety factor) at a reference position $r/a = 0.6$ in the stable region.

In the s-scan, the q-profiles in the linearly unstable region are set to provide conditions for identical linear instabilities. All q-profiles have the same safety factor $q = 1.7$ and magnetic shear $s = 0.43$ at the center of the unstable region ($r/a = 0.35$). In the unstable region, the q-profiles are nearly the same with some small variations due to the method of our q-profile generation. However, the difference in linear growth rate is about 10% of the average at the maximum, and is negligible. Thus, the unstable core region provides a source of virtually identical fluctuation pulses. The q-profiles show differences in the linearly stable region. Using this setup, we can study the changes of turbulence spreading caused by the variation of magnetic shear. The q-profiles in the safety factor scan have the same s-profile with the case of $s = 1.0$ in the s-scan [the black curve in Fig. 2(b)] and cover the range of variation of q-values in the s-scan.

It should be noted that there is no profile control during the simulations. ITG Turbulence is excited by ion temperature gradient, produces heat transport, and ultimately decays as free energy in the gradient is exhausted. However, the turbulence spreading processes occur faster than the turbulence decays. Quantitatively speaking, the ratio of the spreading time to the decay time is $\gamma_{decay}\Delta t_{spread} = 0.1 - 0.5$, where $\gamma_{decay} \equiv I^{-1}\partial I/\partial t$. The penetration of turbulence into the stable region stops before the turbulence in the unstable region decays away. We do observe clear effects of q-profile on turbulence spreading.

Other simulation parameters are set as follows: A concentric circular equilibrium is used with $R_0 = 220$ cm and $a = 70$ cm. Velocities are normalized by $v_{T0} = \sqrt{T_0/m_i} = 3.8 \times 10^7$ cm/s and time by $\tau_s \equiv R_0/v_{T0} = 5.8\,\mu$s, where v_{T0} and $T_0 = 3$ keV are the ion thermal velocity and ion temperature in the center, respectively. A deuterium plasma is assumed. The normalized value of the ion Lamor radius in the center is $\rho_{i0}/a = 1/167$. The fluctuating potential is normalized as $\phi = e\delta\Phi/T_0$. The number of radial grid points is set as $N_\psi = 256$. The range of toroidal mode number is chosen as $[-48, 48]$, for which $|k_\theta \rho_i| \leq 0.7$ at the center of the unstable region ($r/a = 0.35$). We use a medium number of simulation particles (77×10^6 total) corresponding to 100 particles per grid.

B. Analysis of fluctuation intensity transport

To estimate the strength of spreading, we perform fluctuation intensity balance analysis. We adopt a minimal model describing turbulence spreading dynamics by a single evolution equation for local turbulence intensity I as[6,10]

$$\frac{\partial I}{\partial t} = \frac{\partial}{\partial r}\left(D_0 I \frac{\partial I}{\partial r}\right) + \gamma I - \gamma_{NL} I^2. \tag{3}$$

In the linearly stable region of the present setup, the time evolution of dT_i/dr is limited due to absence of a heat source, and the zonal flow shear is small as compared to the linear growth rate. Because of these features, the simplified 1-field model is very likely to be applicable to interpreting our observations. A steady state in the linearly stable region is attained by the balance between fluctuation energy transfer and local linear damping as

$$-\frac{\partial}{\partial r}\left[D_0 I_S(r)\frac{\partial I_S(r)}{\partial r}\right] = \gamma_d I_S(r), \tag{4}$$

where the nonlinear damping is neglected, as compared to the linear damping $\gamma_d < 0$. After measuring information about the turbulence intensity profile in a steady state I_S and γ_d, we can evaluate strength of spreading, i.e., $D_0 I$. If we consider an idealized situation in Fig. 3 for purpose of illustration, the diffusivity of spreading is determined as

$$D_0 I_0 = |\gamma_d| x_0^2/2, \tag{5}$$

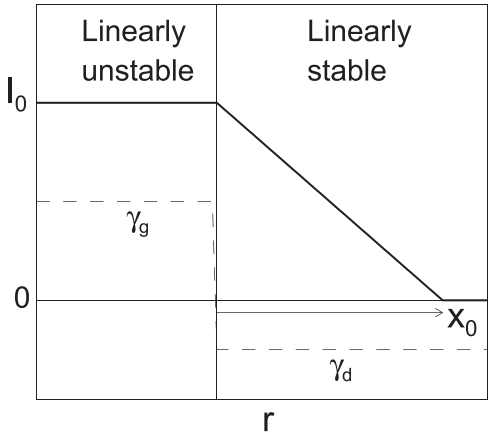

FIG. 3. Idealized profiles of turbulence intensity (solid) in a steady state and linear growth rate (broken).

This article is copyrighted as indicated in the article. Reuse of AIP content is subject to the terms at: http://scitation.aip.org/termsconditions. Downloaded to IP: 132.239.66.163 On: Wed, 14 Jan 2015 19:24:19

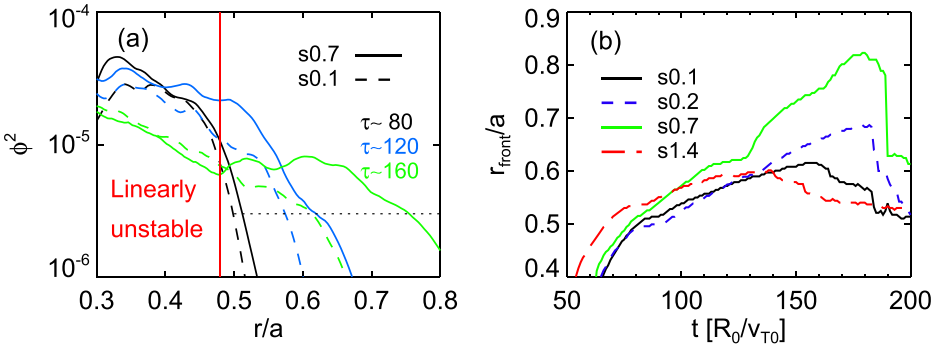

FIG. 4. (a) Time evolution of turbulence intensity profiles and (b) position of the front of turbulence intensity profile in time for different s-profiles. The dotted, horizontal line indicates the specific value of turbulence intensity ($\phi^2 = 3 \times 10^{-6}$), which is used to identify the turbulence front.

from the balance condition in Eq. (4). Here, the intensity of the saturated turbulence I_0 is determined from the interplay among linear excitation, nonlinear damping, and suppression by zonal flow in the linearly unstable region. In fact, this method is very similar to usual transport analysis of thermal diffusivity by measuring heat flux from sources and temperature gradient. Table I draws an analogy between this analysis and usual turbulent transport analysis. In our actual simulations, however, the turbulence intensity profile in the state of saturated spreading is not stationary in time and the intensity gradient has large variation in radius. These features of actual simulations induce a large error bar in the evaluated diffusivity of spreading. In the practical analysis, we use a more sophisticated method to eliminate the effects of the large spatio-temporal variations in the turbulence intensity gradient. The details of the method of spreading estimation are presented in the Appendix.

III. EFFECTS OF *Q*-PROFILE STRUCTURE ON TURBULENCE SPREADING

A. Effects of magnetic shear

We examine turbulence spreading for varying s-profiles in Fig. 2. In what follows, we will consider that the results of this s-scan primarily originate from the variation in magnetic shear, although results include some effects of q-variation in the linearly damping region. The effects of safety factor alone are elucidated in Sec. III B. The time evolution of turbulence intensity profiles is displayed in Fig. 4(a). At each time, we record the radius at which the front of the turbulence envelope pulse of a specified intensity passes through that point. The specific intensity value of the turbulence front, denoted by the dotted line, is about 5% of the nonlinear saturation level, that is, $\phi^2 = 3 \times 10^{-6}$. Figure 4(b) shows the position of the turbulence front in time for different s-profiles. Turbulence penetrates into the linearly stable region until the intensity profile evolves so that the rate of fluctuation energy transfer balances the local linear damping. As s-profile varies, dynamics of spreading shows clear differences.

We measure the penetration depth x_0 from the boundary of the linearly unstable and stable regions at $r/a = 0.48$. Thus, x_0 corresponds to the maximum radius at which the front invades. The penetration depth for the different s-profiles is presented in Fig. 5(a). Turbulence penetration is maximized in the range of modest magnetic shear around $s \sim 0.5$. In the optimal case of $s = 0.7$, a large amount of fluctuation intensity (about 30% of the saturation level) spreads into the stable region. As the magnetic shear deviates from the optimal range, penetration is degraded. The penetration depth sharply decreases for the weak shear regime ($s < 0.3$). A radial correlation length of fluctuation is a proper criterion for the size of the penetration length. We compare the penetration depth with the averaged correlation length of fluctuation, defined as

$$\langle r_c \rangle = \int dV r_c(\theta, \varphi) \phi^2(r, \theta, \varphi) / \int dV \phi^2(r, \theta, \varphi), \qquad (6)$$

where the average is taken in both poloidal and toroidal directions (θ, φ). At every poloidal and toroidal angels, $r_c(\theta, \varphi)$ is estimated from the width of the dominant peak in the k_r power spectrum. We calculate the correlation length $\langle r_c \rangle$ of the fluctuations scattered into the linearly stable region in $r > 0.55a$. The correlation length is averaged over a time period of $\Delta t = 30 - 60\tau_s$, during which the fluctuation front sweeps into the stable region. The correlation length, which is represented by the blue line in Fig. 5(a), shows similar magnetic shear dependence to that of the

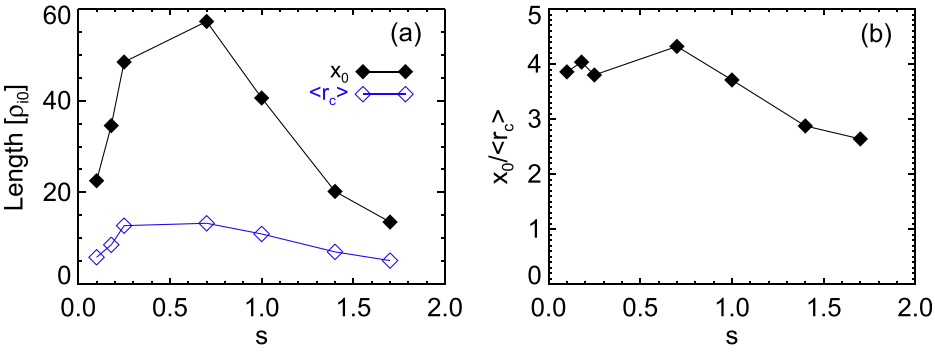

FIG. 5. (a) Penetration depth and radial correlation length as a function of magnetic shear s. (b) The penetration depth x_0 normalized by the correlation length $\langle r_c \rangle$ in Fig. 5(a).

This article is copyrighted as indicated in the article. Reuse of AIP content is subject to the terms at: http://scitation.aip.org/termsconditions. Downloaded to IP: 132.239.66.163 On: Wed, 14 Jan 2015 19:24:19

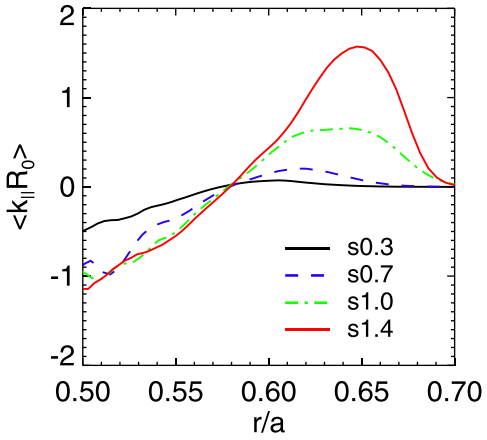

FIG. 6. Radial profiles of the parallel wave number of modes in the linearly stable region of $r/a \sim 0.6$ and at $t \sim 100R_0/v_{T0}$ for different s-profiles.

penetration depth. The penetration depth normalized by the correlation length is displayed in Fig. 5(b) for a direct comparison. The penetration length is much larger than the correlation length, and so corresponds to a meso-scale. Furthermore, we find an additional weak magnetic shear dependence of the normalized penetration depth. As mentioned before, the penetration depth includes the effect of variation of local damping. In what follows, we separate the effect of local damping from penetration depth and estimate strength of spreading for the different s-profiles.

To evaluate the linear damping rates, we compute the profiles of parallel wave number $\langle k_{||}(r)\rangle$ of the modes located in the stable region with $r \sim 0.6a$, which satisfy the condition of $q(0.56a) \leq m/n \leq q(0.60a)$. The parallel wave number decreases for the lower shear cases, as shown in Fig. 6. We note that there are two competing factors determining the parallel wave number as the magnetic shear varies in this study. The lower shear cases have lower q-values, which increase parallel wave numbers. On the other hand, the decrease of the magnetic shear is expected to lower parallel wave numbers. The result in Fig. 6 indicates that the effect of the magnetic shear dominates the direct effect of the q-value in the range of q-profiles used in our s-scan. So, the linear damping rate decreases with decreasing magnetic shear. In this estimation of the linear damping rates, we use the value of $\langle k_{||}\rangle_{rms}$ averaged over a time period of about 20–$40\tau_s$ when the turbulence front passes the radial location of the measurement. The smaller linear damping rates in the lower s cases help the penetration of turbulence.

After separation of the linear damping effect from the penetration depth, we show spreading [i.e., the effective diffusion coefficient $D \equiv D_0 I$ in Eq. (3)] and the square of the turbulence correlation length $\langle r_c\rangle^2$ as a function of magnetic shear s in Fig. 7. We use the intensity of the saturated turbulence in the linearly unstable region for $D \approx D_0 I_0$. The dependency of spreading on s is similar to that of the penetration depth. The maximum diffusivity of spreading is significantly larger than the gyro-Bohm diffusivity $\chi_{GB} \equiv \rho_* \rho_{i0}^2 \omega_c$. This indicates that spreading is a process faster than local diffusion in micro-scales. Recalling the mixing-length rule $D \sim \ell_c^2/\tau_c$, we expect a relation between D and ℓ_c^2. Here, ℓ_c and τ_c are the characteristic length and time scales of turbulence spreading, respectively. A characteristic time, which is obtained by $\tau \equiv \langle r_c\rangle^2/D$, shows a constant value over the range of magnetic shear s, as shown in Fig. 8 by the blue line. This implies that turbulence spreading is directly linked to the correlation length of the fluctuations scattered into the stable region. And the penetration of more correlation lengths in the lower magnetic shear in Fig. 5(b) originates from the help of smaller linear damping rate.

We investigate underlying physical mechanisms of the dependency of spreading on magnetic shear s. In the picture of nonlinear mode-mode interactions, the correlation length of modes having a single helicity can give us a clue. We compute the average correlation lengths of single (m, n) mode, defined as

$$\langle r_{mode}\rangle = \sum_{m,n,\omega>0} \int dV r_{mode,mn} \phi_{mn\omega}^2 \Big/ \sum_{m,n,\omega>0} \int dV \phi_{mn\omega}^2, \quad (7)$$

where the $\phi_{mn\omega}$ is the Fourier component of fluctuating potential in poloidal and toroidal direction (θ, φ) and time, respectively. The fluctuation data analyzed for $\langle r_c\rangle$ are

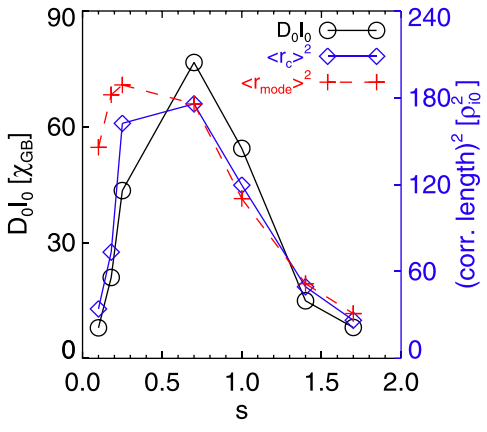

FIG. 7. Diffusion coefficient (black) in the units of gyro-Bohm diffusivity $\chi_{GB} \equiv \rho_* \rho_{i0}^2 \omega_c$ and square of radial correlation lengths as a function of magnetic shear s. The correlation lengths of turbulence eddies $\langle r_c\rangle^2$ (blue) and single spectral mode $\langle r_{mode}\rangle^2$ (red) are averaged in poloidal and toroidal positions and spectral space, respectively.

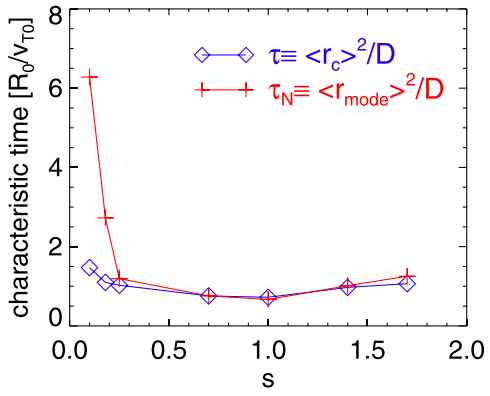

FIG. 8. Characteristic times as a function of magnetic shear, s, estimated by using a mixing-length rule with correlation lengths of eddy (blue) and mode (red). Here, $\langle r_{mode}\rangle$ is the typical correlation length of each spectral components of the total fluctuation, whose correlation length is $\langle r_c\rangle$.

This article is copyrighted as indicated in the article. Reuse of AIP content is subject to the terms at: http://scitation.aip.org/termsconditions. Downloaded to IP: 132.239.66.163 On: Wed, 14 Jan 2015 19:24:19

decomposed into poloidal and toroidal modes and radial correlation lengths of the each mode are estimated. We can interpret $\langle r_{mode} \rangle$ as the typical correlation length of spectral components of the total fluctuation whose correlation length is $\langle r_c \rangle$. The red line in Fig. 7 shows the variation of $\langle r_{mode} \rangle^2$. *We observe an overall increase in* $\langle r_{mode} \rangle$ *with decreasing magnetic shear, whereas D and* $\langle r_c \rangle^2$ *rapidly decrease for low s* ($s \leq 0.3$). *This suggests that, for the low magnetic shear values, the strength of nonlinear interactions becomes weak even for the longer correlation lengths of modes involved in the interactions.* We can introduce a time scale required for nonlinear interactions as $\tau_N \sim \langle r_{mode} \rangle^2 / D$, which is shown in Fig. 8 by the red curve. The divergent behavior of τ_N in low magnetic shear again indicates that the nonlinear interaction slow down. For high shear ($s > 0.7$), the nonlinear interaction time saturates at a lower level and the degradation of the spreading results from the shortening of the mode correlation lengths.

B. Effects of safety factor

We investigate the effects of varying q-values on turbulence spreading with the fixed s-profile of $s = 1.0$. For the q-value scan in Fig. 2, the levels of turbulence and zonal flow in the linearly unstable region show large difference because of the variation of safety factor. The difference of the turbulence source causes the estimation of q-effects difficult. To focus on direct effect of safety factor on spreading, we hold down the variation of the turbulence source by switching off self-generated zonal flow. One of the effects of high q-value is the decrease of linear damping rate due to the dependence $k_{||} R_0 \sim 1/q$. The analysis of simulation data does indicate this trend as presented in Table II, while the linear growth rate and nonlinear damping rate show relatively small changes. Figure 9 shows the penetration depth as a function of the ratio of the linear growth to the damping rate. We find a trend of deeper penetration for higher q-values, i.e., for smaller linear damping rate. The change of the penetration depth is well described by the average value of the estimated D_0's. This indicates that the increased penetration depth for higher q-values results from the changes in local physical processes, i.e., mainly the decrease of linear damping rate. The value of safety factor itself does not affect the efficiency of turbulence spreading much.

In the cases retaining zonal flow, larger zonal flow is driven in the linearly unstable region for the lower safety factor. Thus, turbulence level in the unstable region and penetration depth decrease as safety factor decreases. When we compare the cases with, and without, zonal flow, the penetration depth decreases significantly when zonal flow is retained, for all different q-profiles. This effect of zonal flow in retarding spreading is consistent with the previous result of numerical simulation study in Ref. 18.

TABLE II. Coefficients for the expression of the penetration depth in Eq. (A1), which is estimated from the simulation set for the scan of safety factor.

	$\lvert\gamma_d \tau_s\rvert$	$\gamma_g \tau_s$	$\gamma_{NL} \tau_s$	$\lvert\gamma_g / \gamma_d\rvert$
q2.0	0.25	0.39	2.24×10^3	1.6
q2.5	0.18	0.43	1.89×10^3	2.4
q4.0	0.11	0.47	1.61×10^3	4.3

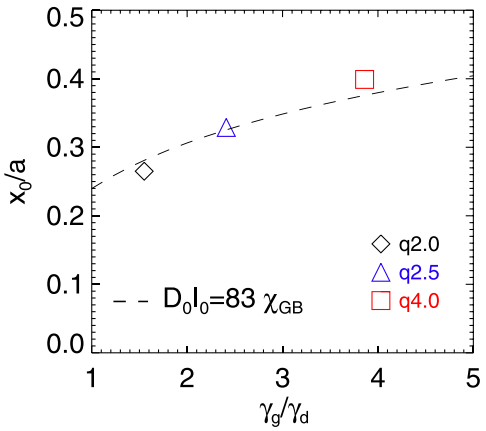

FIG. 9. Penetration depth of turbulence as a function of γ_g / γ_d, the ratio of the linear growth to the damping rate, in the scan of safety factor. The broken line corresponds to an extrapolation of the penetration depth by using Eq. (A1) with the values of diffusion coefficient $D_0 I_0 = 83 \chi_{GB}$ and nonlinear damping rate $\gamma_{NL} = 1.91 \times 10^3 \tau_s^{-1}$, which are the average of the three cases.

IV. CONCLUSIONS AND DISCUSSION

In this paper, we have presented the results of numerical experiments to elucidate the effect of q-profile structure on turbulence spreading. We have examined the propagation of turbulence into a linearly stable region, for different q-profile structures. Turbulence spreading was triggered by an identical instability source in the driving, linearly unstable region. The strength of turbulence spreading was measured by the penetration depth of the turbulence front. We have evaluated the strength of spreading by performing fluctuation intensity balance analysis, using a model intensity evolution equation. This model takes into account the effects of local linear growth/damping, nonlinear damping, and non-local spatial transfer of fluctuation energy by nonlinear interactions. The principal findings of this work are as follows:

1. Turbulence spreading, i.e., the flux of fluctuation energy by nonlinear mode-mode couplings, is strongly affected by magnetic shear s, but is hardly altered by the safety factor q itself, as shown in Figs. 5, 7, and 9.
2. Spreading is maximal in a range of magnetic shear around $s \sim 0.5$, as demonstrated in Figs. 5 and 7. As magnetic shear decreases from a high shear value to this modest value, the spreading is enhanced by the increased mode correlation length.
3. For low magnetic shears ($s < 0.3$), the mode correlation length is large, similar to that of the optimal magnetic shear case, as shown in Fig. 7. However, the time required for the nonlinear interactions to transfer energy increases, as illustrated in Fig. 8. This increase in the characteristic interaction time has a stronger impact on spreading, as compared to the increase of the mode correlation length. Consequently, the overall spreading efficiency drops for low magnetic shear.

This article is copyrighted as indicated in the article. Reuse of AIP content is subject to the terms at: http://scitation.aip.org/termsconditions. Downloaded to IP: 132.239.66.163 On: Wed, 14 Jan 2015 19:24:19

These findings have implications for the interpretation of experiments on ion internal transport barriers (ITBs). ITBs have been produced by tailoring the magnetic shear profile. Weak or negative magnetic shear facilitates enhanced confinement in ITBs.[19–24] The decreased instability drive in weak or negative magnetic shear[31] and the threshold upshift by $E \times B$ flow shear[32] have been recognized to contribute to the enhanced confinement. These are not the only factors relevant to enhanced confinement experiments, however. A dedicated ion transport experiment reveals that the enhanced confinement in weak magnetic shear regime results from mitigated stiffness of the T_i profile rather than increase in the instability threshold.[24] This leads to a significantly higher T_i gradient, well above the levels expected by the threshold upshift. Previous studies based on local, quasi-linear models showed discrepancies in the behavior of stiffness between various experiments. Our novel findings suggest a new mechanism for profile destiffening which incorporates turbulence spreading as an important contributor to the ion heat transport dynamics. Turbulence spreading smooths turbulence intensity—and thus turbulent heat diffusivity—across the boundary between a strongly driven region and a marginally stable region. Such smoothing in the turbulent diffusivity profile degrades confinement in the heating region. The suppression of spreading for weak magnetic shear cause a gap in the turbulence intensity profile across the boundary, and so promotes enhancement of confinement. In other words, the non-local response of plasma profiles to external sources, mediated by turbulence spreading, is diminished by weak magnetic shear. We note that in the experiments of Ref. 24, externally induced toroidal rotation shear V'_φ is shown to be critical to controlling ion heat transport. Although role of externally induced rotation shear is not examined in our work, we expect further fluctuation decorrelation and suppression of spreading by V'_φ for weak magnetic shear due to the increase in the mode correlation length and the interaction time. So, weak shear ($s < 0.3$) promotes locality and fluctuation decorrelation, as well as stability. The synergy between external rotation shear and the magnetic shear dependency of spreading will be clarified in future works.

Future works will aim to address roles of spreading in turbulent transport in various q-profiles including reversed shear q-profiles (the minimum q value at off axis), especially focusing on the following aspects: (1) A quantitative assessment of effects of the interplay of magnetic shear and externally induced toroidal rotation shear on turbulence spreading and transport. (2) Elucidation of effects of zonal flow on nonlinear interactions which induce spreading, and a scan of the effect of zonal flow damping on spreading. (3) A study of the weakening of coupling between flux and local gradient due to spreading in a state of steady, flux-driven turbulence. (4) Investigation of role of spreading in physics of intrinsic rotation through redistribution of residual stress.

ACKNOWLEDGMENTS

We wish to thank the participants in the 2013 Festival de Theorie and 4th APTWG conference for interesting discussions. This work was supported by the World Class Institute (WCI) Program of the National Research Foundation of Korea (NRF) funded by the Ministry of Education, Science and Technology of Korea (MEST) (NRF Grant No.: WCI 2009-001) and by CMTFO funded by the U.S. DOE Grant No. DE-FG02-04ER54738. T. S. Hahm's work was supported by 2014 R&D Program through the National Fusion Research Institute (NFRI) of Korea funded by the Government.

APPENDIX: ESTIMATION OF TURBULENCE SPREADING

The essential constituent in the dynamics of turbulence spreading is fluctuation energy diffusion represented by the diffusion coefficient $D_0 I$. We deduce the coefficient D_0 from the balance between fluctuation energy transfer and local linear damping in the saturation of turbulence spreading as follows. In the present simulation setup, the penetration depth is a representative of the saturated intensity profile in the stable region. An expression for the penetration depth x_0 can be obtained from the steady state solution of Eq. (3) as[10]

$$x_0 = \sqrt{\frac{2D_0}{\gamma_{NL}}} F\left(\left|\frac{\gamma_g}{\gamma_d}\right|\right), \tag{A1}$$

with

$$F(x) \equiv \cosh^{-1}\left(\frac{3}{2}\frac{x}{[4(1+x)]^{1/3}} + 1\right). \tag{A2}$$

Here, $\gamma_g > 0$ and $\gamma_d < 0$ are linear growth and damping rates in the unstable and stable regions, respectively. If we know the local growth and damping rates, the coefficient D_0 can be estimated using the measured x_0 as

$$D_0 = \frac{\gamma_{NL} x_0^2}{2F\left(|\gamma_g/\gamma_d|\right)^2}. \tag{A3}$$

We note that by taking $I_0 = \gamma_g/\gamma_{NL}$ in Eq. (5), the diffusion coefficient in the ideal situation becomes

$$D_0 = \frac{\gamma_{NL} x_0^2}{2|\gamma_g/\gamma_d|},$$

which is quite identical to the precise one. We estimate the local growth and damping rates by the following.

- The linear growth rate in the unstable region can be easily obtained from linear simulations.
- We estimate the linear damping rate in the stable region by employing a fluid model for Landau damping, in which the damping rate of ITG mode is given by[33]

$$\gamma_d = -\frac{\sqrt{2\pi}}{4}|k_{||}|v_{Ti}(2-\eta_i), \tag{A4}$$

for a subcritical $\eta_i < 2$. For the absolute value of $k_{||}$ in Eq. (A4), we take the root-mean-squared value of a $\langle k_{||}(r)\rangle$ profile

This article is copyrighted as indicated in the article. Reuse of AIP content is subject to the terms at: http://scitation.aip.org/termsconditions. Downloaded to IP: 132.239.66.163 On: Wed, 14 Jan 2015 19:24:19

$$\langle k_{||}\rangle_{rms} = \sqrt{\int dV \langle k_{||}(r)\rangle^2 / \int dV}, \quad \text{(A5)}$$

where dV is the volume of toroidal shells. The profile of the parallel wave number of turbulence spectrum is obtained by

$$\langle k_{||}(r)\rangle = \sum_{m,n,\omega>0} \frac{m-nq}{qR_0}\phi^2_{mn\omega}(r) \Big/ \sum_{m,n,\omega>0} \phi^2_{mn\omega}(r). \quad \text{(A6)}$$

For the calculation of $k_{||}$ of damped modes, we count only modes having their own rational surfaces within the stable region.

- Finally, the nonlinear damping rate is estimated from the saturation level of turbulence in the unstable region as $\gamma_{NL} = \gamma_g / I_0(V^2_{ZF})$, because the local nonlinear damping is the saturation mechanism for linear instability in this model. Note that the saturation level of turbulence is also affected by the level of zonal flow, as discussed in Eq. (2). So, the effect of local turbulence suppression by zonal flow is included in γ_{NL}

It is necessary to examine the applicability of the simple 1D model for the analysis of complex gyrokinetic simulation data in 3D toroidal geometry. Our primary concern is whether the functional form of the penetration depth in Eq. (A1) derived from the 1D model can capture the observed trend of turbulence penetration. Let us suppose we selectively change the linear damping rate only in the stable region while keeping the other parameters as the same. If we analyze the simulation data, it should yield an identical D_0 for varying fluctuation levels and penetration depths.

We did perform such a test by imposing ion temperature gradients lower than the linear threshold to change the linear damping rates in the stable region. The q-profile was fixed with the case of $s = 0.7$. Naturally, turbulence penetrates deeper, as the linear damping rate decreases, i.e., as the R_0/L_{Ti} value approaches the threshold of $R_0/L_{Ti}|_{crit} = 4.4$. Table III presents the estimated coefficients for the expression of x_0 in Eq. (A1). Only the linear damping rate varies, while the other coefficients show very slight variations as we intended. Figure 10 shows the penetration depth of turbulence as a function of the ratio of the linear growth to the damping rate. The estimated D_0's for the three cases have very similar values as $D_0 I_0 \sim 75\chi_{GB}$ (see Table III), which supports the validity of applying the 1D model to explain the behavior of turbulence spreading within our work scope. The analytic expression of the penetration depth and our estimation method of local coefficients are suitable for the evaluation of turbulence spreading from the simulation data.

TABLE III. Coefficients for the expression of the penetration depth in Eq. (A1), which is estimated from the simulation set for the linear damping rate scan.

R_0/L_{Ti}	$\lvert\gamma_d\tau_s\rvert$	$\gamma_g\tau_s$	$\gamma_{NL}\tau_s$	$\lvert\gamma_g/\gamma_d\rvert$	$D_0 I_0/\chi_{GB}$
3.1	0.23	0.44	8.0×10^3	2.0	74
3.3	0.19	0.44	8.0×10^3	2.3	75
3.6	0.13	0.44	7.6×10^3	3.3	76

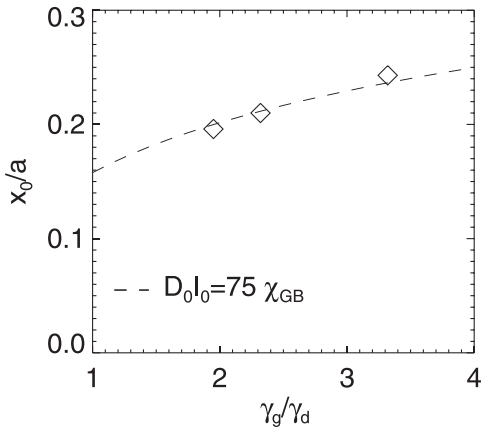

FIG. 10. Penetration depth of turbulence as a function of γ_g/γ_d, the ratio of the linear growth to the damping rate, in the scan of linear damping rate by varying R_0/L_{Ti} in the linearly stable region. The broken line corresponds to an extrapolation of the penetration depth by using Eq. (A1) with the values of diffusion coefficient $D_0 I_0 = 75\chi_{GB}$ and nonlinear damping rate $\gamma_{NL} = 7.8\times10^3\tau_s^{-1}$, which are the averages of the three cases.

[1]C. C. Petty, M. R. Wade, J. E. Kinsey, D. R. Baker, and T. C. Luce, Phys. Plasmas **9**, 128 (2002).
[2]K. W. Gentle, R. V. Bravenec, G. Cima, G. A. Hallock, P. E. Phillips, D. W. Ross, W. L. Rowan, A. J. Wootton, T. P. Crowley, A. Ouroua, P. M. Schoch, and C. Watts, Phys. Plasmas **4**, 3599 (1997).
[3]S. Inagaki, K. Ida, N. Tamura, T. Shimozuma, S. Kubo, Y. Nagayama, K. Kawahata, S. Sudo, K. Ohkubo, and LHD Experimental Group, Plasma Phys. Controlled Fusion **46**, A71 (2004).
[4]T. Estrada, C. Hidalgo, and T. Happel, Nucl. Fusion **51**, 032001 (2011).
[5]X. Garbet, L. Laurent, A. Samain, and J. Chinardet, Nucl. Fusion **34**, 963 (1994).
[6]T. S. Hahm, P. H. Diamond, Z. Lin, K. Itoh, and S.-I. Itoh, Plasma Phys. Controlled Fusion **46**, A323 (2004).
[7]Z. Lin and T. S. Hahm, Phys. Plasmas **11**, 1099 (2004).
[8]L. Villard, P. Angelino, A. Bottino, S. J. Allfrey, R. Hatzky, Y. Idomura, O. Sauter, and T. M. Tran, Plasma Phys. Controlled Fusion **46**, B51 (2004).
[9]T. S. Hahm, P. H. Diamond, Z. Lin, G. Rewoldt, Ö. D. Gürcan, and S. Ethier, Phys. Plasmas **12**, 090903 (2005).
[10]Ö. D. Gürcan, P. H. Diamond, T. S. Hahm, and Z. Lin, Phys. Plasmas **12**, 032303 (2005).
[11]Ö. D. Gürcan, P. H. Diamond, and T. S. Hahm, Phys. Rev. Lett. **97**, 024502 (2006); Phys. Plasmas **13**, 052306 (2006).
[12]V. Naulin, A. H. Nielsen, and J. J. Rasmussen, Phys. Plasmas **12**, 122306 (2005).
[13]X. Garbet, Y. Sarazin, F. Imbeaux, P. Ghendrih, C. Bourdelle, Ö. D. Gürcan, and P. H. Diamond, Phys. Plasmas **14**, 122305 (2007).
[14]Z. H. Wang, P. H. Diamond, Ö. D. Gürcan, X. Garbet, and X. G. Wang, Nucl. Fusion **51**, 073009 (2011).
[15]K. Miki, P. H. Diamond, L. Schmitz, D. C. McDonald, T. Estrada, Ö. D. Gürcan, and G. R. Tynan, Phys. Plasmas **20**, 062304 (2013).
[16]P. H. Diamond and T. S. Hahm, Phys. Plasmas **2**, 3640 (1995).
[17]M. Yagi, T. Ueda, S.-I. Itoh, M. Azumi, K. Itoh, P. H. Diamond, and T. S. Hahm, Plasma Phys. Controlled Fusion **48**, A409 (2006).
[18]W. X. Wang, T. S. Hahm, W. W. Lee, G. Rewoldt, J. Manickam, and W. M. Tang, Phys. Plasmas **14**, 072306 (2007).
[19]Y. Koide, M. Kikuchi, M. Mori, S. Tsuji, S. Ishida, N. Asakura, Y. Kamada, T. Nishitani, Y. Kawano, T. Hatae, T. Fujita, T. Fukuda, A. Sakasai, T. Kondoh, R. Yoshino, and Y. Neyatani, Phys. Rev. Lett. **72**, 3662 (1994).
[20]E. J. Strait, L. L. Lao, M. E. Mauel, B. W. Rice, T. S. Taylor, K. H. Burrell, M. S. Chu, E. A. Lazarus, T. H. Osborne, S. J. Thompson, and A. D. Turnbull, Phys. Rev. Lett. **75**, 4421 (1995).
[21]C. M. Greenfield, K. H. Burrell, J. C. DeBoo, E. J. Doyle, B. W. Stallard, E. J. Synakowski, C. Fenzi, P. Gohil, R. J. Groebner, L. L. Lao, M. A. Makowski, G. R. McKee, R. A. Moyer, C. L. Rettig, T. L. Rhodes, R. I. Pinsker, G. M. Staebler, W. P. West, and the DIII-D Team, Phys. Rev. Lett. **86**, 4544 (2001).

This article is copyrighted as indicated in the article. Reuse of AIP content is subject to the terms at: http://scitation.aip.org/termsconditions. Downloaded to IP: 132.239.66.163 On: Wed, 14 Jan 2015 19:24:19

[22]R. C. Wolf, Plasma Phys. Controlled Fusion **45**, R1 (2003).
[23]P. Mantica, D. Strintzi, T. Tala, C. Giroud, T. Johnson, H. Leggate, E. Lerche, T. Loarer, A. G. Peeters, A. Salmi, S. Sharapov, D. Van Eester, P. C. de Vries, L. Zabeo, and K.-D. Zastrow, Phys. Rev. Lett. **102**, 175002 (2009).
[24]P. Mantica, C. Angioni, C. Challis, G. Colyer, L. Frassinetti, N. Hawkes, T. Johnson, M. Tsalas, P. C. deVries, J. Weiland, B. Baiocchi, M. N. A. Beurskens, A. C. A. Figueiredo, C. Giroud, J. Hobirk, E. Joffrin, E. Lerche, V. Naulin, A. G. Peeters, A. Salmi, C. Sozzi, D. Strintzi, G. Staebler, T. Tala, D. Van Eester, and T. Versloot, Phys. Rev. Lett. **107**, 135004 (2011).
[25]P. H. Diamond, Y.-M. Liang, B. A. Carreras, and P. W. Terry, Phys. Rev. Lett. **72**, 2565 (1994).
[26]P. H. Diamond, S.-I. Itoh, K. Itoh, and T. S. Hahm, Plasma Phys. Controlled Fusion **47**, R35 (2005).
[27]G. Dif-Pradalier, P. H. Diamond, V. Grandgirard, Y. Sarazin, J. Abiteboul, X. Garbet, Ph. Ghendrih, A. Strugarek, S. Ku, and C. S. Chang, Phys. Rev. E **82**, 025401 (2010).
[28]J. M. Kwon, S. Yi, T. Rhee, P. H. Diamond, K. Miki, T. S. Hahm, J. Y. Kim, Ö. D. Gürcan, and C. McDevitt, Nucl. Fusion **52**, 013004 (2012).
[29]T. S. Hahm, Phys. Fluids **31**, 2670 (1988).
[30]T. S. Hahm and W. M. Tang, Phys. Fluids B **1**, 1185 (1989).
[31]R. E. Waltz, G. R. Kerbel, J. Milovich, and G. W. Hammett, Phys. Plasmas **2**, 2408 (1995).
[32]J. E. Kinsey, R. E. Waltz, and J. Candy, Phys. Plasmas **14**, 102306 (2007).
[33]G. W. Hammett and F. W. Perkins, Phys. Rev. Lett. **64**, 3019 (1990).

This article is copyrighted as indicated in the article. Reuse of AIP content is subject to the terms at: http://scitation.aip.org/termsconditions. Downloaded to IP: 132.239.66.163 On: Wed, 14 Jan 2015 19:24:19